Carrier multiplication and separation in systems with strong electron interaction: Photoinduced dynamics of a junction solar cell

W. Koshibae,[1] N. Furukawa,[2] and N. Nagaosa[1,3]

[1]*RIKEN Center for Emergent Matter Science (CEMS), Wako 351-0198, Japan*

[2]*Aoyama-Gakuin University, 5-10-1, Fuchinobe, Sagamihara, Kanagawa 229-8558, Japan*

[3]*Department of Applied Physics, The University of Tokyo, Tokyo 113-8656, Japan*

(Received 16 July 2012; revised manuscript received 24 February 2013; published 19 April 2013)

We examine the real-time photoinduced dynamics of a junction composed of the interacting electron systems and propose a path to enhance the solar-cell efficiency using *multiplication* of electron-hole pairs caused by the electron interaction. The key ingredients for the multiplication are instability and/or metastability of insulator-to-metal transition, and the photoinduced dynamics of the band gap. The band-gap alignment of the junction is also important for efficiency of the carrier generation.

DOI: 10.1103/PhysRevB.87.165126 PACS number(s): 71.10.Fd, 72.40.+w, 78.20.Bh

I. INTRODUCTION

It is an urgent matter to improve the efficiency of the solar cell.[1] For the conventional solar cells, the semiconductors are mostly used, where the energy of absorbed light in excess of the band gap is wasted as a heat. This gives a serious obstacle to improve the performance of the solar cell. A potential idea to overcome this difficulty is the "carrier multiplication."[2–8] This effect is, in principle, based on the electron correlation. In the previous studies,[5–8] therefore, nanosized semiconductors are fabricated because the confinement derives an enhancement of the electron correlation.

On the other hand, the family of Mott insulators and their doped systems are known as the representative of the strongly correlated electronic systems. The systems often show the sensitivity to the external stimuli because of the metastability, i.e., the rich electronic phases with nearly degenerate energies compete with each other.[9] Consequently, even the weak photoirradiation can trigger the insulator-to-metal (IM) transition.[10–13] Note that the band gap of the conventional semiconductor is a fixed quantity which characterizes the electronic state. On the other hand, the band gap (Mott gap) of the strongly correlated electron systems reflects the dynamics of the electronic structure and can be changed by external fields, e.g., photoirradiation. To examine the photoinduced dynamics, we have developed[14] a method for the real-time numerical simulation of a double exchange model[15] where the electrons are interacting with the classical local spins. In that study, we found a considerable *multiplication* of electron-hole (e-h) pairs, i.e., the higher energy (frequency) of incident light derives a larger amount of the multiplication. This will give a path to the high performance solar cell fabricated by transition metal oxides.

In this paper, the path to enhance the efficiency of carrier generation using multiplication of the separated e-h pairs in the interacting electron systems is studied. The essential key ingredients of our proposal are the photoinduced real-time dynamics of the band gap along with the IM electronic phase transition and the focus of an energy window for the emergence of the e-h pair multiplication. First, we show the numerical results of the real-time photoinduced relaxation dynamics on an effective model which is a theoretically designed junction of the interacting electron systems. And, later, in the light of the theoretical results, we summarize the key ingredients for the high-performance solar-cell action.

II. MODEL AND METHOD

We consider a junction system as shown in Figs. 1(a) and 1(b), i.e., the two Mott insulators are connected via tunnel junction, and the "Mott insulator 1" and "Mott insulator 2" correspond to the light absorber and the selective contact to sort out the charge carrier, respectively. The electronic states of a large family of Mott insulators and their doped systems are often accompanied by magnetic ordering. In the magnetically ordered electronic states, the coupled dynamics of the classical spins representing the magnetic moment and quantum electrons describes the interacting electrons because the order parameter behaves as a classical field.[16] In this theory, we adopt the double exchange model[14,15] as the effective Hamiltonian to describe the electronic structure of the Mott insulators. A schematic representation of the model is shown in Fig. 1(c), i.e., the "system 1" and "system 2" are for the Mott insulator 1 and Mott insulator 2, respectively,

$$\hat{H} = \hat{H}_1 + \hat{H}_2 - t' \sum_s \left(\hat{c}^\dagger_{j_a s}\hat{c}_{j_c s} + \text{H.c.}\right) - t' \sum_s \left(\hat{c}^\dagger_{j_b s}\hat{c}_{j_d s} + \text{H.c.}\right), \quad (1)$$

with

$$\hat{H}_\nu = -t_\nu \sum_{j(\nu),s} (\hat{c}^\dagger_{j(\nu)s}\hat{c}_{j(\nu)+1s} + \text{H.c.}) - J_{H,\nu} \sum_{j(\nu),ss'} \hat{c}^\dagger_{j(\nu)s}\hat{c}_{j(\nu)s'}\vec{\sigma}_{ss'} \cdot \vec{S}_{j(\nu)} + J_\nu \sum_{j(\nu)} \vec{S}_{j(\nu)} \cdot \vec{S}_{j(\nu)+1} + J_{N,\nu} \sum_{j(\nu)} (\vec{S}_{j(\nu)} \cdot \vec{S}_{j(\nu)+1})^2 + \text{sgn}(\nu)\Delta V/2 \sum_{j(\nu)} \hat{n}_{j(\nu)},$$

where $\nu = 1,2$ is the index for system 1 and system 2, i.e., $j(\nu)$, t_ν, $J_{H,\nu}$, J_ν, and $J_{N,\nu}$ are the site and coupling constants in system 1 for $\nu = 1$ and in system 2 for $\nu = 2$, respectively, $\text{sgn}(\nu)$ is $+1$ for $\nu = 1$ and -1 for $\nu = 2$, and $\hat{n}_{j(\nu)} = \sum_s \hat{c}^\dagger_{j(\nu)s}\hat{c}_{j(\nu)s}$. The sites j_a and j_b (j_c and j_d) are arbitrarily chosen nearest-neighboring sites from system 1 (system 2). The indices s and s' are for the electron spin, and the

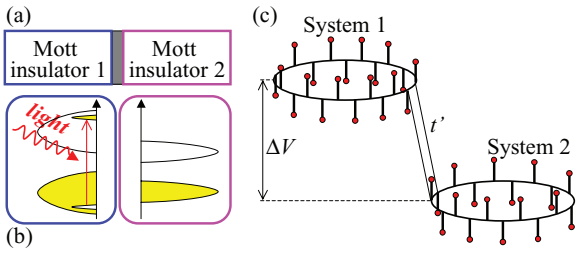

FIG. 1. (Color online) Schematic representation of the junction system. (a) Two Mott insulators are connected via tunnel junction (gray area). (b) The electronic state is shown by the density of states (DOS). The yellow area is occupied by electron. The left panel represents an excited electronic state by a light irradiation. (c) The "junction" system composed of the double exchange models. Two of the sites in system 1 are connected to those of system 2 via hopping matrix element, t'.

components of $\vec{\sigma}$, i.e., σ^x, σ^y, and σ^z, are Pauli matrices. The local spins, $\vec{S}_{j(\nu)}$'s, are taken to be the classical vectors with a magnitude S, and $\hat{c}^\dagger_{j(\nu)s}$ and $\hat{c}_{j(\nu)s}$ are the creation and annihilation operators for the quantum electrons. The quantum electron couples with the classical local spin via $J_{H,\nu}$. The accent $\hat{}$ is used to distinguish the quantum operators and classical variables. In Fig. 1, the stick with a red dot represents a local spin. The two systems, system 1 and system 2, are connected by the hopping matrix element of electron t'. The potential difference ΔV is also introduced.

Here, let us summarize the scheme of the numerical calculation:[14] the Hamiltonian Eq. (1) is expressed to be

$$\hat{H} = \hat{H}_{\rm el} + H_S,$$

with

$$\begin{aligned}\hat{H}_{\rm el} = &-\sum_\nu t_\nu \sum_{j(\nu),s} (\hat{c}^\dagger_{j(\nu)s}\hat{c}_{j(\nu)+1s} + {\rm H.c.}) \\ &-\sum_\nu J_{H,\nu} \sum_{j(\nu),ss'} \hat{c}^\dagger_{j(\nu)s}\hat{c}_{j(\nu)s'}\vec{\sigma}_{ss'}\cdot\vec{S}_{j(\nu)} \\ &- t'\sum_s (\hat{c}^\dagger_{j_a s}\hat{c}_{j_c s} + \hat{c}^\dagger_{j_b s}\hat{c}_{j_d s} + {\rm H.c.}) \\ &+\sum_\nu {\rm sgn}(\nu)\Delta V/2 \sum_{j(\nu)} \hat{n}_{j(\nu)}\end{aligned}$$

and

$$H_S = \sum_\nu J_\nu \sum_{j(\nu)} \vec{S}_{j(\nu)}\cdot\vec{S}_{j(\nu)+1} + \sum_\nu J_{N,\nu}\sum_{j(\nu)} (\vec{S}_{j(\nu)}\cdot\vec{S}_{j(\nu)+1})^2,$$

i.e., $\hat{H}_{\rm el}$ involves creation and annihilation operators of quantum electron, while H_S does not. We numerically calculate the time ($\tilde{T}$) evolution of the electronic state $|\Phi(\tilde{T})\rangle$ and the local spins $\{\vec{S}_{j(\nu)}(\tilde{T})\}_{j(\nu)}$ for the small time increment $\tilde{T} \to \tilde{T} + \Delta\tilde{T}$ on the finite size system. In system 1, the effect of *light* is introduced by the time-dependent vector potential $A(\tilde{T})$ into the hopping matrix element, i.e., $t_1 \to t_1 e^{iA(\tilde{T})}$. Therefore, the Hamiltonian is also time dependent through the vector potential $A(\tilde{T})$ and the local spins $\{\vec{S}_{j(\nu)}(\tilde{T})\}_{j(\nu)}$. In the beginning, we put $A(\tilde{T}=0) = 0$ and a set of local spins $\{\vec{S}_{j(\nu)}(\tilde{T}=0)\}_{j(\nu)}$. The Hamiltonian $\hat{H}_{\rm el}(\tilde{T}=0)$ is numerically diagonalized in a form

$$\hat{H}_{\rm el}(\tilde{T}=0) = \sum_{\ell=1}^{L_1+L_2} E_\ell(\tilde{T}=0)\hat{\phi}^\dagger_\ell(\tilde{T}=0)\hat{\phi}_\ell(\tilde{T}=0),$$

i.e., the fermion operator is expressed to be

$$\hat{\phi}^\dagger_\ell(\tilde{T}=0) = \sum_\nu \sum_{j(\nu)s} a^*_{j(\nu)s\ell}(\tilde{T}=0)\hat{c}^\dagger_{j(\nu)s}$$

for an eigenstate of ℓth level $E_\ell(\tilde{T}=0)$. We fill up the eigenstates from the lowest energy level to the energy level being the total number of electrons N_e on the finite size system, i.e.,

$$|\Phi(\tilde{T}=0)\rangle = \prod_{l=1}^{N_e} \hat{\phi}^\dagger_\ell(\tilde{T}=0)|0\rangle$$

and take this state as an initial electronic state. The Landau-Lifshitz-Gilbert (LLG) equation is introduced for the equation of motion of local spins:

$$\dot{\vec{S}}_{j(\nu)}(\tilde{T}) = -\vec{h}_{{\rm eff},j(\nu)}(\tilde{T}) \times \vec{S}_{j(\nu)}(\tilde{T}) - \alpha_\nu \vec{S}_{j(\nu)}(\tilde{T}) \times \dot{\vec{S}}_{j(\nu)}(\tilde{T}),$$

where α_ν ($\nu = 1$ is for system 1 and $\nu = 2$ is for system 2) is the Gilbert damping constant[17] and

$$\vec{h}_{{\rm eff},j(\nu)}(\tilde{T}) = \langle\Phi(\tilde{T})| - \partial\hat{H}(\tilde{T})/\partial\vec{S}_{j(\nu)}(\tilde{T})|\Phi(\tilde{T})\rangle.$$

By integrating the LLG equation, we calculate the time evolution of the local spins, i.e., $\{\vec{S}_{j(\nu)}(\tilde{T})\}_{j(\nu)} \to \{\vec{S}_{j(\nu)}(\tilde{T} + \Delta\tilde{T})\}_{j(\nu)}$. By putting the new local spin texture $\{\vec{S}_{j(\nu)}(\tilde{T} + \Delta\tilde{T})\}_{j(\nu)}$ and $A(\tilde{T} + \Delta\tilde{T})$, we obtain the instantaneous electronic Hamiltonian $\hat{H}_{\rm el}(\tilde{T} + \Delta\tilde{T})$ at time $\tilde{T} + \Delta\tilde{T}$. The time evolution of the electronic state during the small time increment $\Delta\tilde{T}$ is given by

$$|\Phi(\tilde{T} + \Delta\tilde{T})\rangle = \prod_{p=1}^{N_e} \hat{\Phi}^\dagger_p(\tilde{T} + \Delta\tilde{T})|0\rangle,$$

with

$$\hat{\Phi}^\dagger_p(\tilde{T} + \Delta\tilde{T}) = e^{-i\hat{H}_{\rm el}(\tilde{T}+\Delta\tilde{T})\Delta\tilde{T}/\hbar}\hat{\Phi}^\dagger_p(\tilde{T})e^{i\hat{H}_{\rm el}(\tilde{T}+\Delta\tilde{T})\Delta\tilde{T}/\hbar}$$

and $\hat{\Phi}^\dagger_p(\tilde{T}=0) = \hat{\phi}^\dagger_p(\tilde{T}=0)$. We successively calculate the time evolution of the local spin and electronic states in total for the small time increment $\tilde{T}$ to $\tilde{T} + \Delta\tilde{T}$, and examine the photoinduced electron-spin coupled dynamics. Due to the first-order nature of the IM transition in the real systems,[9–13] the typical length scale of the time evolution of the electronic state discussed is of the order of 5–10 lattice sites. Therefore, the one dimensionality and small size of the present system does not disturb the essential part of the phenomenon. Also the excitation density of the electron hole need not be so large as in the simulation since this electronic process occurs rather locally and hence will remain unchanged even if we increase the size of the system.

III. RESULTS

We consider the half-filled case, i.e., the number of electrons is equal to the number of sites. The biquadratic exchange interaction of the local spins in the Hamiltonian Eq. (1) gives a metastability between ferromagnetic-metallic (FM)

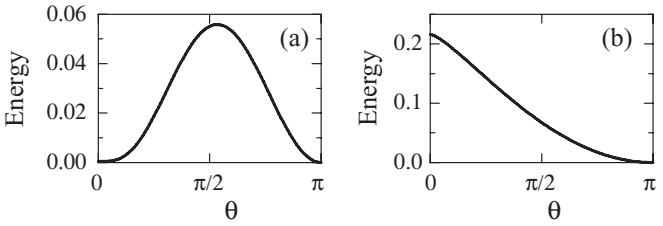

FIG. 2. (a) Metastability of the system 1. A parameter set $\{t_1 = 1.0,\ SJ_{H,1} = 1.0,\ S^2J_1 = -0.119,\ S^4J_{N,1} = -0.085,\ L_1 = 20\}$ is used. The lowest energy per site is measured from the ground state as a function of the angle between neighboring local spins in the isolated system 1, i.e., in the case with $t' = 0$. In this case, the FM ($\theta = 0$) and the AFI ($\theta = \pi$) states are almost degenerate and divided by a potential barrier. (b) The same as (a) but for system 2, and a parameter set $\{L_2 = 20, t_2 = 0.5, SJ_{H,2} = 1.0, S^2J_2 = S^4J_{N,2} = 0\}$ is used. In this case, the AFI ($\theta = \pi$) state is stabilized.

and antiferromagnetic-insulating (AFI) states for $J_{N,\nu} < 0$. Figure 2(a) shows the metastability of the isolated system 1, i.e., the lowest energy per site within two-sublattice consideration is plotted as a function of the angle between neighboring local spins θ at half-filling with the number of sites $L_1 = 20$ and a parameter set $\{t' = 0,\ t_1 = 1.0,\ SJ_{H,1} = 1.0,\ S^2J_1 = -0.119,\ S^4J_{N,1} = -0.085\}$. (Hereafter, t_1 is a unit of energy in this paper.) In this numerical condition, the FM ($\theta = 0$) and the AFI ($\theta = \pi$) states are almost degenerate, and we can examine the photoinduced IM transition on the system 1. On the other hand, we take a parameter set $\{t' = 0,\ t_2 = 0.5,\ SJ_{H,2} = 1.0,\ S^2J_2 = S^4J_{N,2} = 0.0\}$ with the number of sites $L_2 = 20$ for system 2. In this case, at half-filling, the AFI state is stabilized enough and is the unique ground state [see Fig. 2(b)].

Figure 3 shows the numerical result for $L_1 = L_2 = 20$ with $t' = 0.1$, $\Delta V = 1.0$. For the relaxation dynamics, we take the Gilbert damping constants $S\alpha_1 = 0.01$ and $S\alpha_2 = 1.0$, and $S = 1$ is used. Here, the dimensionless time $T = (t_1/\hbar)\tilde{T}$ is defined, so that the unit $\hbar/t_1$ is typically $\sim 10^{-15}$ s assuming $t_1 = 0.4$ eV. In the real-time simulation, the instantaneous Hamiltonian is diagonalized in a form

$$\hat{H}_{\rm el}(T) = \sum_{\ell=1}^{L_1+L_2} E_\ell(T)\hat{\phi}^\dagger_\ell(T)\hat{\phi}_\ell(T),$$

i.e., the fermion operator

$$\hat{\phi}^\dagger_\ell(T) = \sum_\nu \sum_{j(\nu)s} a^*_{j(\nu)s\ell}(T)\hat{c}^\dagger_{j(\nu)s}$$

is for an eigenstate of ℓth level $E_\ell(T)$ at time T. We numerically solve $E_\ell(T)$ and $a_{j(\nu)s\ell}(T)$, and calculate the local density of states (DOS) of the site $j(\nu)$ at T by

$$d_{j(\nu)}(\varepsilon,T) = -(1/\pi){\rm Im}\sum_s \langle 0|\hat{c}_{j(\nu)s}[\varepsilon - \hat{H}_{\rm el}(T) + i\delta]^{-1}\hat{c}^\dagger_{j(\nu)s}|0\rangle$$
$$= -(1/\pi){\rm Im}\sum_{\ell s} |a_{j(\nu)s\ell}(T)|^2/[\varepsilon - E_\ell(T) + i\delta].$$

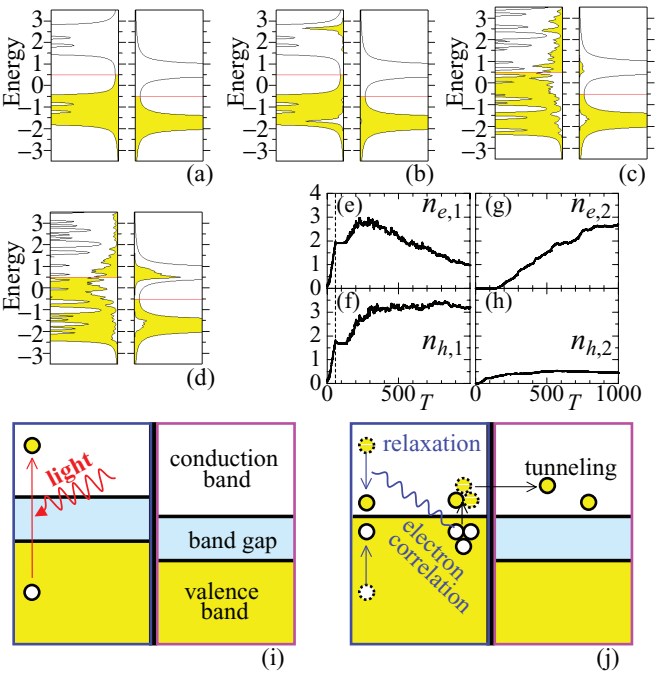

FIG. 3. (Color online) Time evolution of the electronic structure of the junction system. The DOS D_ν's (see text) as a function of energy are shown in (a)–(d), i.e., horizontal and vertical axes are DOS (in arbitrary unit) and energy. The electron occupancies are also shown by yellow area. The figures (a), (b), (c), and (d) are the results for system 1 (left panel) and system 2 (right panel) at $T = 0$, 30, 200, and 500, respectively. The red horizontal lines, which are at $\Delta/2$ in system 1 and at $-\Delta/2$ in system 2, show the centers of mass of the energy bands in each system. Figures (e) and (f) [(g) and (h)] are the number of excited electrons and holes of system 1 [system 2] as the function of T, respectively. Figures (i) and (j) are the schematic representations of the time evolution. The band gap of system 2 plays a role of "filter" to sort out the *multiplied* electrons from system 1.

Using the local DOS, the total DOS in system 1 (system 2) is calculated by

$$D_\nu(\varepsilon,T) = (1/L_\nu)\sum_{j(\nu)} d_{j(\nu)}(\varepsilon,T),$$

with $\nu = 1$ ($\nu = 2$). We define the local electron-occupation number at T by

$$n_{j(\nu)\ell}(T) = {\rm Re}\left[\sum_s a_{j(\nu)s\ell}(T)\langle\Phi(T)|\hat{\phi}^\dagger_\ell(T)\hat{c}_{j(\nu)s}|\Phi(T)\right],$$

which holds the relation

$$\sum_\nu\sum_{j(\nu)} n_{j(\nu)\ell}(T) = \langle\Phi(T)|\hat{\phi}^\dagger_\ell(T)\hat{\phi}_\ell(T)|\Phi(T)\rangle$$

being the electron occupancy of ℓth level at T. Using $n_{j(\nu)\ell}(T)$, we calculate the electron occupancy of ℓth level in system 1 (system 2) by

$$n_{\ell,\nu}(T) = \sum_{j(\nu)} n_{j(\nu)\ell}(T),$$

with $\nu = 1$ ($\nu = 2$). To measure the number of excited electrons and holes in system 1, we calculate

$$n_{e,1}(T) = \sum_{E_\ell(T) > \Delta V/2} n_{\ell,1}(T)$$

and

$$n_{h,1}(T) = \sum_{E_\ell(T) < \Delta V/2} [1 - n_{\ell,1}(T)],$$

respectively. In the same way,

$$n_{e,2}(T) = \sum_{E_\ell(T) > -\Delta V/2} n_{\ell,2}(T)$$

and

$$n_{h,2}(T) = \sum_{E_\ell(T) < -\Delta V/2} [1 - n_{\ell,2}(T)]$$

are also defined for system 2.

Figures 3(a)–3(d) show the time evolution of the electronic state by the DOS D_ν's with electron occupancy by the Lorentzian with $\delta = 0.05$. The time T dependence of e-h pairs is shown by $n_{e,1}$, $n_{e,2}$, $n_{h,1}$, and $n_{h,2}$ in Figs. 3(e)–3(h). The initial state is an AFI one.[18] At $T = 0$, both system 1 and system 2 have the insulating band gaps $2SJ_{H,1}$ in system 1 and $2SJ_{H,2}$ in system 2, respectively, and the lower energy bands are completely filled by electrons but the upper ones are empty in each system as shown in Fig. 3(a). In system 1, the effect of *light* is introduced by the time-dependent vector potential $A(T)$ into the hopping matrix element, i.e., $t_1 \to t_1 e^{iA(T)}$. In the early stage, we have applied $A(T) = A_0 \sin(\omega T)$ in a period $0 < T < T_f$ and turned off the *light* at T_f when the number of excited electrons $n_{e,1}$ reaches 2.0, and later $T_f < T$, $A(T) = 0$. The frequency ω is tuned for the energy difference between the second highest and the second lowest energy levels of the AFI state on the finite size system.[19] The energy of the incident *light* is much larger than the band gap $2SJ_{H,1}$. For Fig. 3, $A_0 = 0.1$ and $T_f = 58.70$. As seen in Figs. 3(b), 3(e), and 3(f), the e-h pairs are created by the *light* during $0 < T < T_f$.[20] For a period just after turnoff the *light*, $T_f < T \lesssim 135$, $n_{e,1}$, and $n_{h,1}$ almost stay around the values at T_f and, later, those increase. This is the multiplication of e-h pairs in this system. The corresponding electronic structure is shown in Fig. 3(c). As seen in the left panel of this figure, the insulating band gap in system 1 almost closes, and at around the center of mass of the band indicated by the red line, we found a considerable multiplication of e-h pairs. Note that an amount of the initially excited e-h pairs during the initial stage $0 < T < T_f$ is still remaining at the high-energy region, i.e., the multiplication occurs at the *low-energy* window. For $T \gtrsim 200$, $n_{e,1}$ decreases. At the same time, $n_{e,2}$ increases. The result shows that the e-h pairs are separated and the electrons (holes) accumulate into system 2 (system 1). The separation of e-h pairs suppresses the e-h pair recombination. Therefore, $n_{h,1}$ saturates for $T \gtrsim 200$.

The photoinduced dynamics of the electronic state is schematically shown in Figs. 3(i) and 3(j): the electronic state in system 1 is excited by *light* at the first stage. Because of the metastability of system 1, the relaxation dynamics results in the collapse of the insulating band gap in system 1. During the gap-closing transition, multiplication of e-h pairs mainly occurs at the *low-energy* window in system 1. Because the low-energy window for holes in system 1 is in the band gap in system 2, the holes in system 1 cannot penetrate into system 2. Finally, the e-h pairs are separated, i.e., the electrons accumulate into system 2 but the holes remain in system 1. It is important to note that the amount of the collected electrons and holes are larger than that of initially created e-h pairs by *light* irradiation.

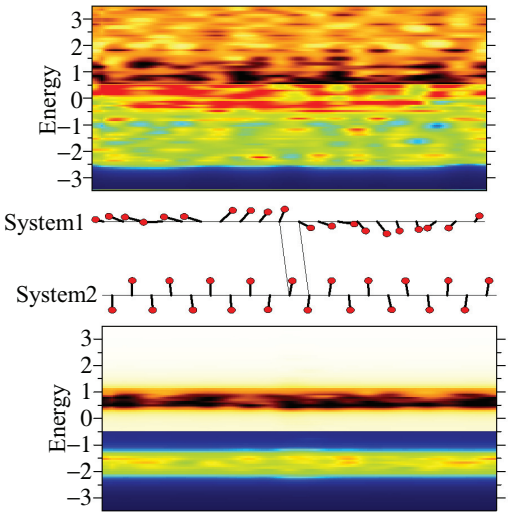

FIG. 4. (Color online) Band diagram and spin structure at $T = 500$. The upper and lower color maps show the electronic structures of the systems, system 1 and system 2, respectively. Different color tones are used above and below the center of mass of the energy bands for the states of excited electrons and holes. The light-yellow and dark-blue regions correspond to the forbidden bands. The orange and light-green areas show the conduction and valence bands, respectively. The black (red) area in the conduction (valence) band represents the distribution of excited electrons (holes). The lattice and spin structures are presented between the band diagrams.

The gap-closing transition is a consequence of the real-time dynamics of the electronic and the local spin structures. A typical dynamic state is shown in Fig. 4, i.e., the local spin structure, the band diagram, and the distribution of excited electrons and holes calculated from $n_{j(\nu)\ell}$ at $T = 500$. In this theory, the electron-electron interaction is mapped into the spin-electron coupled dynamics,[14] and this dynamics is essential for the multiplication of e-h pairs. The photoexcited electrons drive the active dynamics of the local spins. The active dynamics of the local spins also couples with the band structure. In the time evolution, the growing active spin-electron coupled dynamics becomes critical and, finally, the band gap collapses with a drastic change of spin structure.

Now let us focus on the role of IM transition and band alignment of junction to optimize the parameters for the higher efficiency of e-h creation and separation. A key for the multiplication of an e-h pair along with IM transition is the "energy window," i.e., our numerical results suggest that the multiplication of an e-h pair is accelerated by the IM transition and mainly occurs at the low-energy window [see Figs. 3(c) and 3(d)]. Here, we examine the several cases which

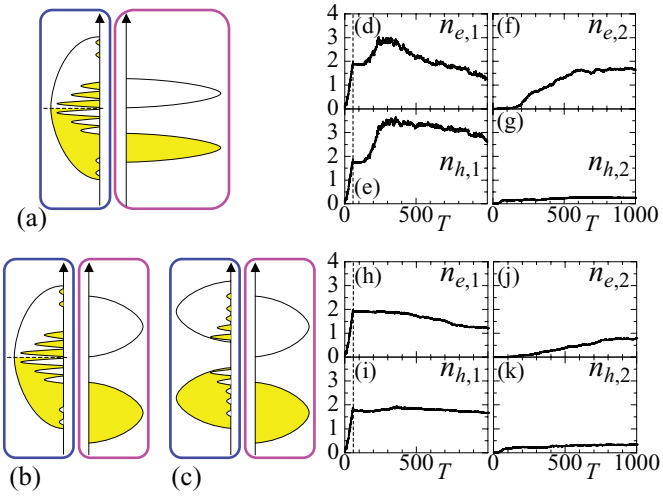

FIG. 5. (Color online) Theoretical design for high-efficiency solar-cell action (see text). (a)–(c) Schematic representation of the electronic structure in the relaxation dynamics. Figures (d)–(g) are the numerical results with a parameter set where $t_2 = 1.0$ and other parameters are the same as those in the case of Figs. 3(e)–3(h). In the case of Figs. (h)–(k), a parameter set where $S^2 J_1 = S^4 J_{N,1} = 0.0$, $t_2 = 1.0$, and other parameters are the same as those in the case of Figs. 3(e)–3(h).

are schematically summarized in Figs. 5(a)–5(c): Fig. 5(a) describes a snapshot of DOS for the case where the gap closes due to the photoexcitation in system 1 (left). A portion of the initially excited e-h pair is remaining at the high energy region and the multiplied e-h pairs are generated at a low-energy window. To focus the low-energy window, the conduction band of the system 2 (right) with a high DOS is arranged in Fig. 5(a), which corresponds to the optimal case for the carrier generation studied in Fig. 3. Figure 5(b) is similar to Fig. 5(a), but the conduction band of the system 2 is broad with lower DOS, i.e., this condition is not satisfied well on the low-energy window of the multiplication in system 1 in comparison to the case of Fig. 5(a). Figure 5(c) represents the case without IM transition in system 1.

Figures 5(d)–5(g) show the numerical results with $t_2 = 1.0$, which is twice as large, while the other parameters are the same as those for Fig. 3. The comparison between Figs. 3 and Figs. 5(d)–5(g) tells us the difference between Figs. 5(a) and 5(b). In the case of Figs. 5(d)–5(g), the multiplication of e-h pairs with the IM transition occurs in system 1; however, the amount of collected electrons $n_{e,2}$ is smaller than that in Fig. 3. This is because of the difference of the DOS in system 2 at the low-energy window, e.g., see Figs. 5(a) and 5(b): the smaller DOS at the low-energy window results in a smaller transition rate of multiplied electrons from system 1 to system 2. It is also noted that the remaining excited electrons in system 1 cause the e-h pair recombination. This leads to the decrease in $n_{h,1}$ at $T \sim 1000$ [see Fig. 5(e) and compare with Fig. 3(f)].

For Figs. 5(h)–5(k), $S^2 J_1 = S^4 J_{N,1} = 0.0$ and $t_2 = 1.0$ are used and the other parameters are the same with those for Fig. 3. In this case which corresponds to Fig. 5(c), the AFI state is stabilized enough without metastability in system 1, and neither IM transition nor remarkable multiplication of e-h pairs occurs. Therefore, a small amount of $n_{e,2}$ is obtained at $T \sim 1000$. The comparison between Figs. 3(e)–3(h) and Figs. 5(h)–5(k) shows that the effect of carrier multiplication results in a three times or more larger amount of collected electron and hole.

Here, let us discuss the efficiency of the *light*-to-electric energy conversion within this calculation. During $0 < T < T_f$, the *light* is applied to excite the electronic state, and the energy absorbed from the light (E_f) is defined as the excitation energy of the particle-hole pair just after T_f. Because the transfer integral $t' = 0.1$ between system 1 and system 2 is much smaller than those within each system, one can approximately define the chemical potentials independently. Therefore, ΔV can be regarded as the "voltage drop" of the designed solar cell in our model. A measure of the electric power generation (W) is the product of ΔV and the amount of transferred electron $n_{e,2}$ at the system 2. By using the value of $n_{e,2}$ at $T = 1000$ where the relaxation is almost saturated, we estimate the efficiency W/E_f as follows: $W/E_f \sim 33\%$ in the case of Fig. 3, $W/E_f \sim 20\%$ in the case of Figs. 5(d)–5(g), and $W/E_f \sim 10\%$ in the case of Figs. 5(h)–5(k). Thus it is concluded that the multiple carrier generation due to electron correlation offers an efficient way to improve the energy conversion rate in the solar cell.

IV. DISCUSSION

We have examined the junction system composed of light absorber and selective contact; the latter one is introduced to collect the charge carrier. Our theoretical results indicate the strategy to enhance the number of collected electrons and holes using multiplication of e-h pairs: (1) metastability for IM transition in the light absorber; (2) matching of band gap between the light absorber and selective contact; (3) high DOS at the *low-energy* window of the selective contact. To (1), the metastability and/or instability of the IM transition can be controlled by[9] external magnetic field, external electric field, chemical carrier doping, chemical pressure, strain effect by heterojunction and superlattice, and so on, i.e., there are a large number of control parameters. The dynamics during the IM transition, i.e., the gap-closing dynamics, is responsible for the multiplication of e-h pairs. Near the phase boundary of the first-order phase transition, the characteristic real-time dynamics is expected as a steady state under the light irradiation: the insulating electronic state melts into a metallic one by light irradiation. The melting is the time evolution of the spatially inhomogeneous electronic state rather than the instantaneous and simultaneous transition in the whole area.[14] Depending on the metastability of the insulating and metallic state, the areas with IM transition locally appear and disappear successively, and the time-dependent inhomogeneous mixed state by different phases forms the steady state. In a large family of the transition metal oxides, e.g., vanadates, nickelates, and manganites, this situation of metastability often occurs. The IM transition along with the characteristic dynamics is of crucial importance for the mass production of photocarrier by the multiplication. The multiplication mainly occurs at the low-energy window. To take advantage by the carrier multiplication, the conduction band of the selective

contact must be focused on the low-energy window. This is of importance for the design of the junction. The band gap of the selective contact plays a role of "filter" to sort out the multiplied carriers from the light absorber, by tuning of the band-gap alignment. For this purpose, the strongly correlated system is not always required for the selective contact.

It is noted that the mechanism of solar-cell action due to IM transition discussed in the present paper is rather robust against the electron-phonon interaction which is a serious issue in the conventional semiconductor systems. Our numerical results show that the band gap closes in the early stage (typically within the order of small fraction of picosecond) of the photoinduced real-time dynamics of electronic state, and carrier multiplication occurs and is enhanced with the band-gap closing. Once the metallic electronic state is achieved the electron-phonon interaction is suppressed due to the screening.[21] Usually the electron-phonon interaction becomes active after this electronic process occurs, typically of the order of 0.1–1 ps. Therefore, the mechanism of carrier multiplication presented in this study is expected to be not disturbed by the electron-phonon interaction.

V. SUMMARY

In conclusion, we have examined the multiplication of e-h pairs in the interacting electron systems by the real-time photoinduced dynamics. The metastability of the interacting electron system brings about the characteristic dynamics of the band gap and results in the multiplication of electron-hole pairs. The multiplication mainly occurs at a low-energy window. This is of importance for the design of the junction system to maximize the carrier generation. A future experimental study using transition metal oxides, whose band lineup has been investigated,[22] is highly desired.

ACKNOWLEDGMENTS

The authors are grateful to Y. Tokura and M. Kawasaki for useful discussions. This work is supported by KAKENHI (Grants No. 21244053, No. 21360043, and No. 24360036), a High-Tech Research Center project for private universities from MEXT, the "K" computer project of Nanoscience Program, JST-CREST, SICP-(Joint Research Type) from JST, NEDO, and Funding Program for World-Leading Innovative R & D on Science and Technology (FIRST Program).

[1] M. I. Hoffert, K. Caldeira, G. Benford, D. R. Criswell, C. Green, H. Herzog, A. K. Jain, H. S. Kheshgi, K. S. Lackner, J. S. Lewis, H. D. Lightfoot, W. Manheimer, J. C. Mankins, M. E. Mauel, L. J. Perkins, M. E. Schlesinger, T. Volk, and T. M. L. Wigley, Science **298**, 981 (2002).

[2] P. Würfel, Sol. Energy Mater. Sol. Cells **46**, 43 (1997); P. Würfel, A. S. Brown, T. E. Humphrey, and M. A. Green, Prog. Photovoltaics **13**, 277 (2005).

[3] J. H. Werner, R. Brendel, and H.-J. Queisser, Appl. Phys. Lett. **67**, 1028 (1995).

[4] A. Luque and A. Martí, Phys. Rev. B **55**, 6994 (1997).

[5] M. Califano, A. Zunger, and A. Franceschetti, Appl. Phys. Lett. **84**, 2409 (2004).

[6] R. D. Schaller and V. I. Klimov, Phys. Rev. Lett. **92**, 186601 (2004).

[7] R. D. Schaller, M. Sykora, J. M. Pietryga, and V. I. Klimov, Nano Lett. **6**, 424 (2006).

[8] M. C. Beard, K. P. Knutsen, P. Yu, J. M. Luther, Q. Song, W. K. Metzner, R. J. Ellingson, and A. J. Nozik, Nano Lett. **7**, 2506 (2007).

[9] M. Imada, A. Fujimori, and Y. Tokura, Rev. Mod. Phys. **70**, 1039 (1998).

[10] K. Miyano, T. Tanaka, Y. Tomioka, and Y. Tokura, Phys. Rev. Lett. **78**, 4257 (1997); M. Fiebig, K. Miyano, Y. Tomioka, and Y. Tokura, Science **280**, 1925 (1998).

[11] S. Iwai, M. Ono, A. Maeda, H. Matsuzaki, H. Kishida, H. Okamoto, and Y. Tokura, Phys. Rev. Lett. **91**, 057401 (2003).

[12] D. Polli, M. Rini, S. Wall, R. W. Schoenlein, Y. Tomioka, Y. Tokura, G. Cerullo, and A. Cavalleri, Nat. Mater. **6**, 643 (2007).

[13] Y. Okimoto, X. Peng, M. Tamura, T. Morita, K. Onda, T. Ishikawa, S. Koshihara, N. Todoroki, T. Kyomen, and M. Itoh, Phys. Rev. Lett. **103**, 027402 (2009).

[14] W. Koshibae, N. Furukawa, and N. Nagaosa, Phys. Rev. Lett. **103**, 266402 (2009); Europhys. Lett. **94**, 27003 (2011).

[15] P.-G. de Gennes, Phys. Rev. **118**, 141 (1960).

[16] P. W. Anderson, *Basic Notions of Condensed Matter Physics*, Advanced Book Program (Benjamin/Cummings, Menlo Park, CA, 1984).

[17] The magnitude of the Gilbert damping constant is typically in the range $1.0 \gtrsim \alpha \gtrsim 0.01$, e.g., A. P. Malozemoff and J. C. Slonczewski, *Magnetic Domain Walls in Bubble Materials* (Academic Press, London, 1979).

[18] In order to mimic the thermal fluctuation, we introduce a random tilting of each spin from the perfect antiferromagnetic configuration up to 0.1 rad, which corresponds to the state with an excitation energy of $\sim 0.0003t$ from the ground state.

[19] Typical strongly correlated electron systems with photoinduced IM transition have[9–13] the insulating gap of $\sim$1 eV (charge transfer gap in most cases), and the photon energy of two times as large as the insulating gap is enough to trigger the IM transition. This is taken into account in the numerical simulation, i.e., the energy of initially created e-h pairs by light irradiation is about twice of insulating gap $2SJ_{H,1}$ in "system 1." In this paper, to demonstrate the effect of "carrier multiplication" along with the IM transition, we use a high-frequency incident light for the photoexcitation. This effect is enhanced for larger energy of the incident light, and becomes weaker for smaller frequency and is missing with the frequency being equal to the band gap (see also Ref. 14).

[20] The holes created by the *light* irradiation in "system 1" can penetrate into "system 2," but the excited electrons cannot because of the band alignment. Therefore, $n_{e,1}$ and $n_{h,1}$ are not the same in the period $0 < T < T_f$.

[21] As a textbook for the effect of electron-phonon interaction in metals, see J. R. Schrieffer, *Theory of Superconductivity* (Benjamin, New York, 1964).

[22] M. Nakamura, A. Sawa, J. Fujioka, M. Kawasaki, and Y. Tokura, Phys. Rev. B **82**, 201101(R) (2010).